Pergamon

Journal of Structural Geology, Vol. 19, No. 11, pp. 1405 to 1417, 1997

PII: S0191-8141(97)00066-7
0191-8141/97 $17.00 + 0.00

Study of strain and partial-melt transfer in a banded migmatite

DAVID C. TANNER* and JAN H. BEHRMANN

Geologisches Institut, Universität Freiburg, Albertstrasse 23b, D-79104, Freiburg, Germany

(*Received* 2 *June* 1997; *accepted in revised form* 20 *August* 1997)

Abstract—An attempt is made to analyse in detail the strain and area change around the tip of a foliation-parallel leucosome. Strain is determined in the mesosomes above and below the leucosome and the melanosome, in both the *XZ* (foliation and lineation parallel) and *YZ* (foliation parallel, lineation perpendicular) planes, using the following methods: March analysis of biotite orientation fabric; Fry method of zircon position fabric; and R_f/ϕ' method using cordierite grain outlines. In addition, March analysis of the orientation of sillimanite inclusions within the cordierite grains helps confirm the last method. Area change is measured by determining the population density of zircon around the leucosome in the *XZ* plane. The amount of material lost can account for the area gain in the leucosome and we suggest the sample, at the observed scale, was 'closed' in terms of melt movement. The results are used to construct tentative strain paths for the various components of the migmatite. Evidence suggests the leucosome was filled by true melt. Fluid deformation of the leucosome melt is demonstrated by the orientations of zircons. © 1997 Elsevier Science Ltd.

INTRODUCTION

Migmatites are closely linked with the mobilization of partial melts in the continental crust (Mehnert, 1968), and are often considered as the source rocks of anatectic granitoids. However, the exact nature of the processes that lead to the separation of quartzo-feldspathic bodies from the host rock is still under debate. Two models have been proposed: subsolidus metamorphic diffusion and anatexis (e.g. Loberg, 1963; Robin, 1979; Olsen, 1982; Sawyer and Barnes, 1988; Maaløe, 1992). In an attempt to address this problem, research has mainly concentrated on migmatite petrology and 'chemical mass balancing' (e.g. Ashworth, 1979; Mehnert and Büsch, 1982), quantitative models of material separation (e.g. McKenzie, 1984, 1985; Lindh and Wahlgren, 1985), melting experiments (e.g. Jurewicz and Watson, 1985; Dell'Angelo and Tullis, 1988) and textural observations (e.g. Karlsson and Wahlgren, 1982; McLellan, 1983, 1988). Reviews of 'the migmatite problem' are given by Mehnert (1968), Atherton and Gribble (1983) and Ashworth (1985).

In this paper we consider the deformation and associated material transfer in a banded migmatite. We use microstructural observations and quantitative analysis of microscopic fabrics to test the hypothesis that leucosomes are the products of partial melting (anatexis) and local melt migration. We also investigate the question of whether material transfer takes place in an open or closed system, and attempt to characterize the kinematics of the emplacement of the leucosome.

*Author to whom correspondence should be addresssed at: Brueckenhofstrasse 3, D-34587 Felsberg-Altenbrunslar, Germany.

REGIONAL AND GEOLOGICAL SETTING

The object of study is a migmatitic gneiss ('Zeilengneise') of the Moldanubian Supergroup on the western margin of the Bohemian Massif in Central Europe. The rocks of the Moldanubian Supergroup were regionally metamorphosed during the late Carboniferous (Davis and Schreyer, 1962; Grauert *et al.*, 1973; Teufel, 1988) in a high-temperature–low-pressure regime. Peak metamorphic grade in study area was around 650–800°C at 3–4 kbar (Blümel, 1982, 1986; Kleemann, 1992; Tanner *et al.*, 1993; Schuster, 1994). An earlier high-pressure metamorphic event of unknown age is only preserved locally in competent calc-silicate boudins and rigid minerals such as garnet (Wagener-Lohse and Blümel, 1986; O'Brien, 1989; Schuster, 1994; Tanner and Behrmann, 1995), but in the gneiss considered in our study the low-pressure event has completely overprinted the mineral assemblages and older grain shape and crystallographic fabrics by mineral recrystallization and neoblastesis.

The rocks of the Moldanubian Supergroup have recorded an intense polyphase deformation which can be divided into six stages (Tanner and Behrmann, 1995; Tanner, 1996). The first and second deformation fabrics are correlated to the first metamorphism and are rarely preserved. The regional, penetrative foliation relates to the third deformation event and is synchronous with the thermal maximum of the low-pressure metamorphism, dated by uranium–lead monazite radiometric ages at 335–330 Ma (Teufel, 1988; Grauert *et al.*, 1990). Widespread and intensive migmatization is associated with this main-phase (third) deformation event (Tanner, 1996). Between 1 and 20 Ma elapsed before the region cooled to less than 600°C, according to geospeedometry analysis of zoned garnets (Behrmann *et al.*, 1994; O'Brien

and Vrána, 1995). Potassium–argon biotite cooling ages range from 320 to 308 Ma (Davis and Schreyer, 1962; Kreuzer *et al.*, 1989; Mielke, 1990).

FIELD OBSERVATIONS

The sample locality lies close to the political border between Germany and the Czech Republic, near the village of Stadlern (49°30′30″ 12°37′05″). The exposed rocks in this area, typical of the whole region, are monotonous metasedimentary gneisses. Thin (< 1 cm) quartz-feldspar bodies (termed leucosomes after Mehnert, 1962, 1968), spaced 0.5–2 cm apart, lie completely parallel to the D_3 foliation. These are *stromatitic* leucosomes after Foye (1916) and Niggli and Huber (1943). The leucosomes reach dimensions of up to 1–2 m in length in the plane of the foliation.

The D_3 deformation event of the Moldanubian produced a steep to subvertical penetrative foliation, together with a steeply NW- to N-plunging stretching lineation (Tanner, 1996). At this locality, the D_3 foliation strikes 009° and dips 65°E (Fig. 1). The D_3 stretching lineation (consisting of biotite and sillimanite) pitches 78°N on the foliation plane. There is no evidence of D_1 or D_2 fabrics in this outcrop. The fourth, fifth and sixth deformation stages of the Moldanubian gneisses involved large-scale upright folding and local shearing, but structures attributable to these phases of deformation are not seen at the sampling locality.

The vorticity number was measured in the XZ plane in an outcrop 3 km from the sample location in this work, using the method of Passchier (1990). The method involved determining the different deformation histories of variously oriented veins (leucosomes). Because of the lack of information in one orientation, the vorticity number could only be estimated to be between 0.5 and 0.8 (Tanner, 1996).

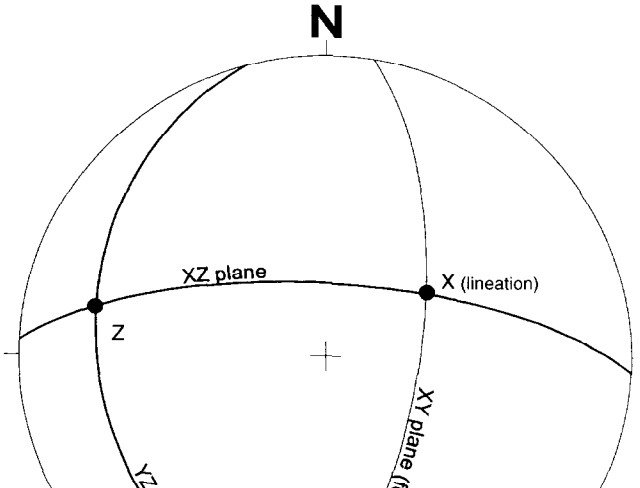

Fig. 1. Equal-area, lower-hemisphere stereographic projections showing the orientation of the D_3 fabric axes from this sample. The bold great circles are the planes analysed in this study.

Regional D_3 strain measurements, mostly using the Fry and R_f/ϕ' methods (see below) on various markers, demonstrate that most strain ellipsoids are close to the plane-strain geometric form (Tanner and Behrmann, 1995). Strain ratios, measured in the YZ and XY planes, are as high as 3–3.5 and 3, respectively, but this probably only reflects different increments of strain as the different markers progressively grew during D_3 (Tanner, 1996).

For convenience, the orientation axes used in this work are fabric axes, where X is parallel to the stretching lineation and the XY plane is parallel to the foliation plane (Fig. 1). Strain measurements (see below) proved these also to be the bulk strain axes. The terms 'above' and 'below' the leucosome used from now on are thus relative to the Z direction. All measurements were made in either the XZ or the YZ plane.

PETROGRAPHIC DESCRIPTION

This investigation is particularly concerned with the rectangular volume (dimensions: $X = 25$ mm; $Y = 15$ mm; $Z = 12$ mm) directly around the tip of a stromatitic leucosome (Fig. 2). Using the terminology of Ashworth (1985), the area can be subdivided into the following.

(1) The leucosome itself, which contains coarse leucocratic minerals with subordinate biotite (Fig. 3a and Table 1).

(2) A region of melanocratic minerals, such as cordierite and biotite, evident *only* below the leucosome, which will be termed the melanosome.

(3) The statistically proven (Tanner, 1996), relatively metamorphically more mature (Flinn, 1969), regions of gneiss above and below the leucosome, which will be known as the upper and lower mesosomes, respectively.

(4) In the XZ plane the leucosome terminates to the right, leaving an area of mesosome (Figs 2 & 3b). This region has been further divided into three subareas for one strain analysis and the area change analysis (see later), which laterally correspond to the upper mesosome, leucosome–melanosome and the lower mesosome.

The leucosome is composed of quartz, alkali-feldspar (microcline) and plagioclase with minor biotite flakes (Table 1 and Fig. 3a). The quartz has slightly undulose extinction, but shows no other signs of deformation. Both feldspars and biotite grains have well-developed crystal faces, although the latter have a much smaller grain size (Table 1).

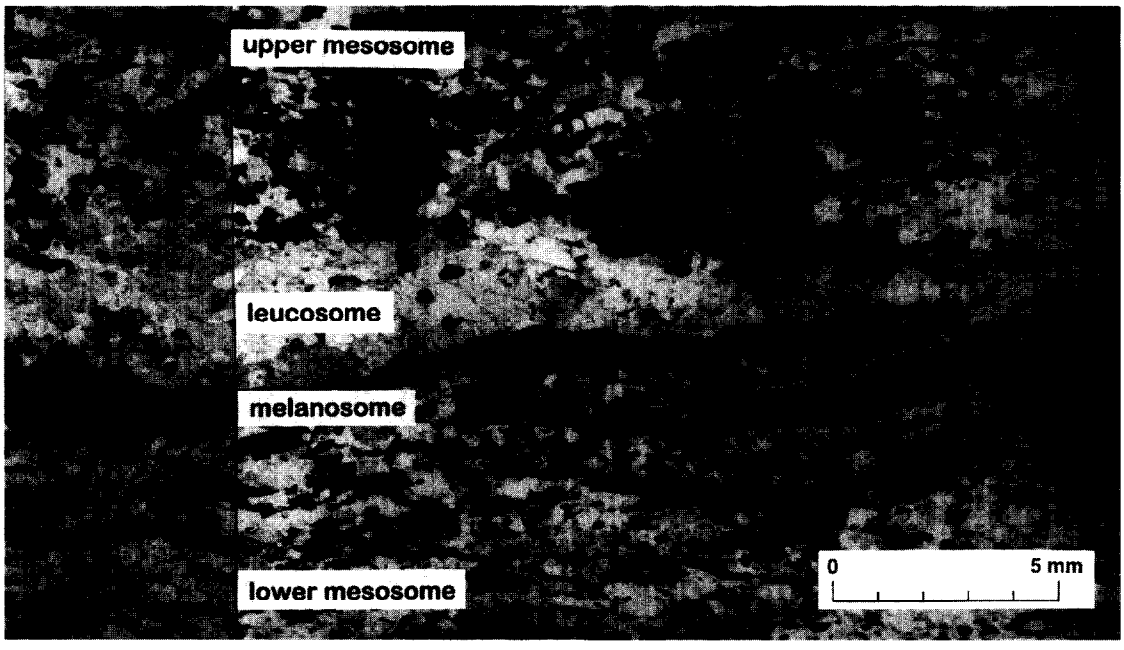

Fig. 2. Photomicrograph of the *XZ* section of the studied sample, in plane-polarized light. Note tapering of the leucosome to the right.

The mesosomes contain quartz, plagioclase, alkali-feldspar (microcline), biotite, cordierite and sillimanite (Table 1 and Fig. 3b). A spaced (1–2 mm) foliation and weak stretching lineation are produced by banding of biotite and quartz-feldspar layers, and by a shape-preferred alignment of all the minerals (Fig. 2). Quartz grains are strongly subgrained and demonstrate evidence of grain-boundary migration. Some quartz and feldspar grains show dynamic recrystallization by subgrain rotation. Cordierite grains have clearly defined cores filled with sillimanite crystals, while the rims are clear with occasional inclusions of biotite. Pinitization of the cordierite is minimal. Sillimanite is also found within microcline and plagioclase grains.

In the melanosome, cordierite and biotite are most conspicuous, with some quartz (Table 1). In general, the grain size of the leucosome is coarser than that of the mesosomes, although the latter displays a narrower range of grain sizes.

STRAIN ANALYSES

Strain analyses are not commonly carried out in granulitic tectonites because of the polyphase nature of the deformation, insecurity about the stability and length of the existence of the marker minerals, and the unknown behaviour of minerals at such temperatures and pressures; i.e. if they were passive or active during the deformation (cf. Ramsay and Huber, 1983, pp. 107–125; Oertel, 1985). Nevertheless, we attempted such a strain analysis while aware of these problems. We used three different methods on four different types of markers (minerals) from the studied sample, which allowed us to overcome some of the above reservations. The method and the results of each method, together with the relative merits of the markers will be separately discussed in detail below.

The March method on biotite orientation

This method of determining strain values from the orientation of tabular or planar objects was first described by March (1932). For planar objects, the stretch in any direction is given by the inverse cube root of the normalized density of an object population with that direction. The method assumes that the objects had a random orientation before deformation, and deformed as a statistical sample of passive markers. A useful description with geological examples is given by Oertel (1985).

In the gneiss studied here, there is no record of any previous fabric. Biotite, cordierite, alkali-feldspar and possibly plagioclase all grew during the low-pressure metamorphism. However, we still cannot assume that the newly formed mineral fabric was completely randomly orientated at any time. An originally preferred orientation of the markers will thus tend to over- or underestimate the real strain (see also the discussion of the R_f/ϕ' method).

We used biotite grains as markers for this analysis for the upper and lower mesosomes, melanosome and leucosome. The orientations of individual grains were measured by determining the position of the (001) cleavage using a U-stage microscope. The (001) cleavage is parallel to the long axes of biotite in this sample (e.g. Fig. 3b). As the timing of the biotite crystallization cannot be rigorously determined, strain estimates will

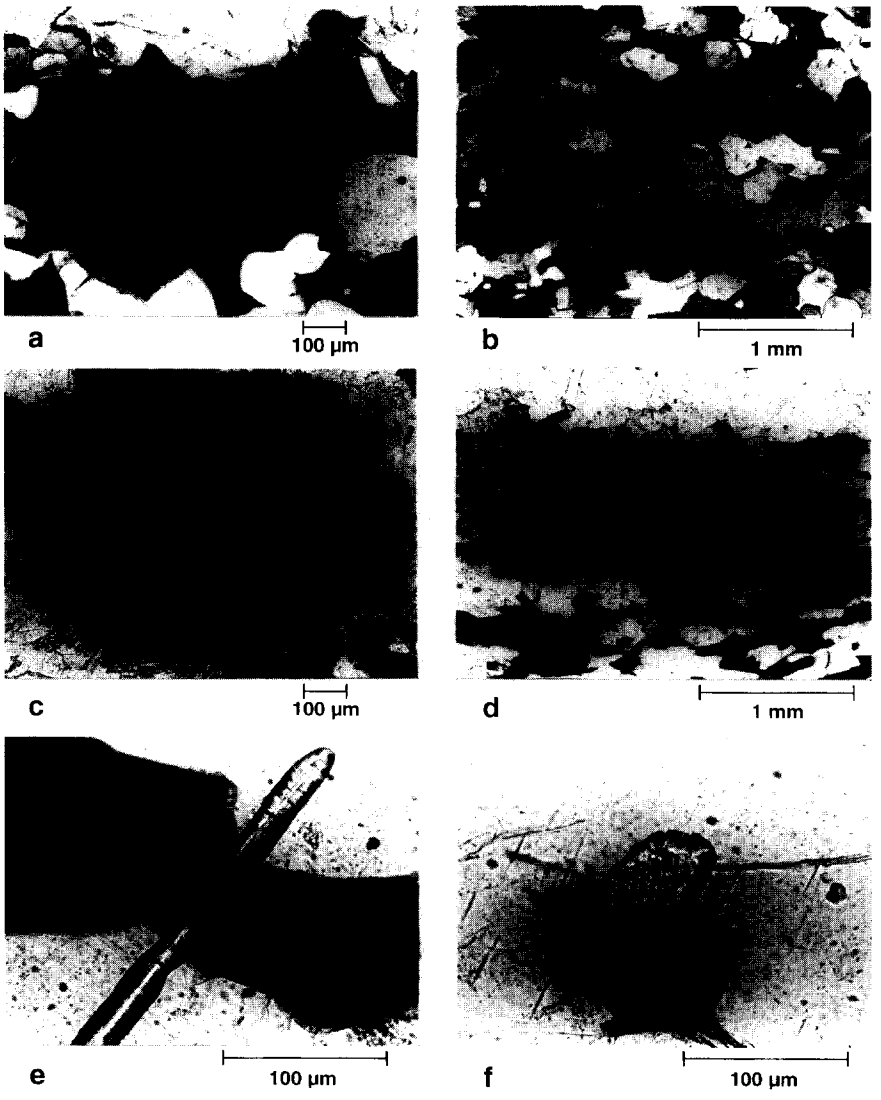

Fig. 3. Photomicrographs of textures and minerals in *XZ* plane view. (a) Texture of the leucosome, subeuhedral biotite, plagioclase and microcline grains with interstitial quartz. Note the widespread 120° triple-point boundaries. Crossed polars. (b) Texture of mesosome. Dispersed biotite forming spaced foliation with microcline, plagioclase and quartz. Note the large cordierite on the left-hand side with a grey, sillimanite-filled core. Crossed polars. (c) Cordierite grain (grain 1, Fig. 6), upper mesosome. Core of tightly spaced, near-randomly orientated, sillimanite inclusions. Plane-polarized light. (d) Cordierite grain (grain 2, Fig. 6), melanosome; leucosome is visible along the top edge of the photograph. Note the core of sillimanite inclusions with strongly preferred orientation and the highly elliptical shape of the cordierite grain. Plane-polarized light. (e) Typical zircon grain of the leucosome. Note the well-formed faces and high length/width ratio. Plane-polarized light. (f) Typical zircon grain in the mesosome. Zircon is in contact with biotite and surrounded by microcline. Plane-polarized light.

Table 1. Area percentage and mean area (in the *XZ* plane) of minerals in the leucosome, mesosomes and melanosome

	Leucosome		Mesosomes		Melanosome	
Mineral	Area (%)	Mean grain area ($\times 10^4$ μm^2)	Area (%)	Mean grain area ($\times 10^4$ μm^2)	Area (%)	Mean grain area ($\times 10^4$ μm^2)
Plagioclase	25.0	2.74	9.9	1.76	—	—
Quartz	47.4	3.29	16.7	1.33	1.3	0.07
Alkali-feldspar	25.0	1.73	28.5	1.95	—	—
Biotite	2.0	0.68	28.7	1.11	13.4	0.67
Cordierite	—	—	15.8	1.81	85.3	4.56
Mean/σ_n		2.11/1.0		1.59/0.3		0.73/0.6

σ_n, standard deviation.

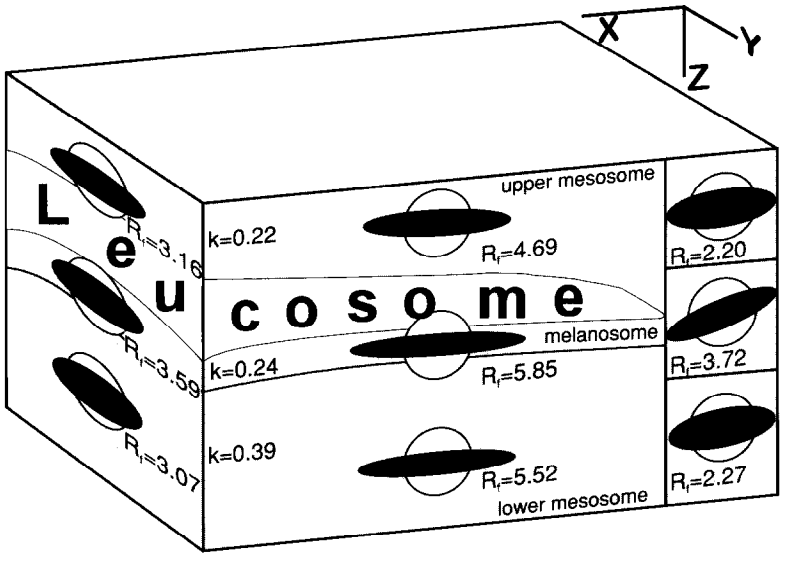

Fig. 4. Results of the Fry strain analysis on zircon position fabric for the various areas of the migmatite on the *XZ* and *YZ* planes. See the text for a description of areas.

only reflect the increment of D_3 deformation that postdates crystallization.

The Fry method on zircon position

The position fabric of zircon was used to determine strain ratios using the Fry technique (Fry, 1979). This centre-to-centre technique relies on the homogeneous strain of markers during a deformation and requires an originally random distribution of markers to produce meaningful results. If data are unevenly distributed or not enough points are chosen (see Fry, 1979 for complete requirements of the method) an ellipse is not produced at the centre of the plot. In addition, we used an additional nearest-neighbour analysis (PODI—normalized population against direction; Unzog, 1992) to check the results of the Fry analysis. A successful result was produced only if both types of analysis correlated.

Owing to the high population density of zircon grains in this gneiss, it was possible to determine domainal strains in the *YZ* and *XZ* planes in the upper and lower mesosomes, melanosome and in the *XZ* plane in three subareas to the right of the leucosome tip, laterally equivalent to the upper mesosome, leucosome–melanosome and lower mesosome (Fig. 4).

In the leucosome there is clear evidence of new euhedral zircon growth (Fig. 3e), but zircons found in the mesosomes and melanosomes belong to only one generation that are all subrounded or faceted and short prisms (Fig. 3f; see discussion below). Zircons are found as inclusions in all mineral phases and are not concentrated within biotites or on grain boundaries.

The centre-points of zircons were traced onto transparent paper from a Petroscope® and then digitized. It was not necessary to incorporate the size of the zircon markers into the analysis to normalize the data (Erslev, 1988; Erslev and Ge, 1990) as the zircon grain size is far smaller than their spacing. The data were analysed using the computer program STRAIN (Unzog, 1992).

The R_f/ϕ' method on cordierite outlines

Cordierite grain outlines were used to determine strain using the R_f/ϕ' method (Ramsay, 1967; Dunnet, 1969; Lisle, 1985). This method has the strength that the initial marker ellipticity (R_i) can be determined and thus the real strain (R_s) can be separated from the finite marker ellipticity (R_f). Only the deformation of the marker itself is calculated; the matrix strain will only be the same if both marker and matrix have the same viscosities (Lisle, 1985). In addition to the R_i calculation check, inconsistent data will not match the best-fit curves (Ramsay and Huber, 1983; Lisle, 1985).

Cordierite grain outlines (e.g. Fig. 3c & d) were analysed, in both the *XZ* and the *YZ* planes, in the lower mesosome, upper mesosome and melanosome. In addition, the shapes of the sillimanite-filled cores of the cordierites (e.g. Fig. 3c & d) in the same three areas were analysed. Outlines were drawn from the Petroscope®, digitized and then examined using the STRAIN program (Unzog, 1992).

The March method on sillimanite preferred orientations within cordierite grains

Sillimanite crystal orientations were measured in three cordierite grains in the *XZ* plane, using the March method (see above) for needle-shaped objects, to check the R_f/ϕ' strain estimates on cordierite core outlines (see above). The sillimanite within the cordierite grains is

Table 2. Results of the March strain analysis on biotite fabric

Area	Strain ratios (R_f)			Flinn k value
	X/Z	X/Y	Y/Z	
Upper mesosome	1.83	1.15	1.59	0.25
Leucosome	1.24	1.05	1.18	0.28
Melanosome	2.17	1.18	1.84	0.21
Lower mesosome	2.35	1.32	1.77	0.42

fibrolitic, with a needle-like habit (Fig. 3c & d). Cordierite cores have up to 40% volume sillimanite, and no other mineral phase is present. Sillimanite crystal long axes were traced from a magnified Petroscope® image, digitized and then grouped by orientation.

RESULTS OF THE STRAIN ANALYSES

March method on biotite orientation

Table 2 shows the strain values obtained from all the migmatite areas using the March method on biotite. Biotite recorded almost no strain in the leucosome. Considering the penetrative foliation in the mesosomes and melanosomes, it is surprising that the strain values derived from these areas are so low. Biotite was clearly affected by partial-melting and recrystallization processes within the rock, so it is possible that many generations of the phase were measured in this analysis, which produced a 'mixed' strain value. All the strain ellipsoids are of the apparently flattening-strain type (Table 2) and strain appears to be higher in the lower mesosome and melanosome than in the upper mesosome.

Fry method on zircon distribution

All the analyses of the zircon fabric from all areas produced interpretable results. Fry plots and PODI analysis correlated within 5% for both strain ratios and orientations of the principal axes. Strain ratios in the XZ and YZ planes for the Fry method on zircon position are shown in Fig. 4. Generally, strain ratios are high, over 3 in the YZ plane and over 4.6 in the XZ plane. Strain is highest in the melanosome. Although laterally equivalent (with respect to the foliation) to the upper mesosome, melanosome and lower mesosome, the three zones to the right of the leucosome tip show distinctly less strain. This aspect will be discussed later. The long axes of all strain ellipses are oriented subparallel ($\pm 5°$) to the foliation, except the subarea to the right of the leucosome–melanosome, where the long axis of the ellipse is oriented at 25° to the foliation trace. The k values for all migmatite areas are less than 0.39 (Fig. 4).

As pointed out above, we consider these zircons to be either detrital and/or metamorphic. Detrital zircon cores with metamorphic overgrowths have been reported from the Moldanubian gneisses (Tondar and Troll, 1992). Thus, with respect to the D_3 deformation, the zircons will have recorded most, if not all, the strain.

R_f/ϕ' method on cordierite outlines

The R_f/ϕ' method on cordierite shapes (Fig. 5) gives strain ratios which fall between those derived from the biotite and zircon fabrics. The melanosome records the highest strain. In the XZ plane, strain in the upper mesosome is higher than in the lower mesosome, but the reverse situation occurs in the YZ plane. Strain ratios measured from the cordierite core outlines are less than

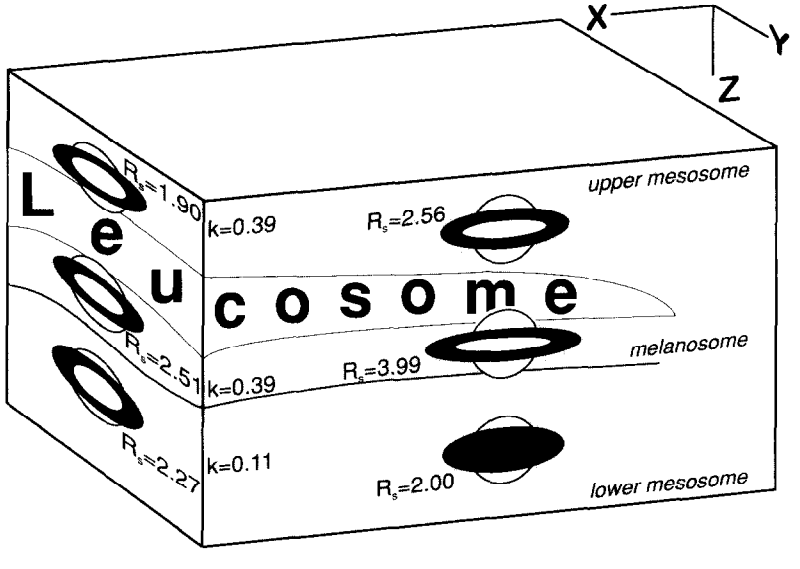

Fig. 5. Results of the R_f/ϕ' strain analysis on the cordierite outline and the core outline shape for the various areas of the migmatite on the XZ and YZ planes. Dark grey ellipses, outer shapes of cordierite; white ellipses, sillimanite-filled cores of cordierite. R_s values are for grain outlines only.

or equal (within a margin of error of less than 5%) to the strain ratios of the whole grain shape (Fig. 5). R_i values for all areas and sections analysed were lower than 1.5.

Cordierite was a reactive phase in this gneiss; it is the breakdown product of garnet and was probably involved in partial-melting reactions (Tanner *et al.*, 1993). At granulite-facies conditions, cordierite can grow by diffusion-controlled processes. Nevertheless, Fediuk (1974), Skrotzki and Siegesmund (1992) and Skrotzki *et al.* (1992) have reported dislocation creep as the dominant deformation mechanism in cordierite from Moldanubian gneisses. At high temperatures, the micromechanics of intracrystalline deformation in cordierite are similar to that of quartz (van Roermund and Konert, 1990; Skrotzki and Siegesmund, 1992). The preferred orientations of sillimanite needles within the cordierite suggest that intra-crystalline plasticity is an important process in the generation of the cordierite shape fabric, because if the grain shape had been formed by diffusion-controlled processes preferred orientation of inclusions would not be expected. Moreover, the R_i values from this analysis (< 1.5) indicate that the cordierites were nearly spherical before deformation.

March method on sillimanite orientation within cordierite grains

March analysis of the orientations of sillimanite needles within three cordierite grains are shown in Fig. 6. Sillimanite long axis orientations fit the predicted standard distribution curve (March, 1932). Strain ratios determined by this method are in accordance with the shape of the individual grain (Fig. 6), within an error of less than 8%.

The nearly random orientation of sillimanite crystals in the only slightly deformed grain 1 (Fig. 3c) suggests that there is no inherited strain from earlier deformation phases. This analysis demonstrates that both the cordierite and the sillimanite are syn- or pre-D_3. Hence, the proposed post-kinematic and replacement nature of the sillimanite in cordierite in these gneisses (as suggested by Voll, 1960) is not supported here.

ESTIMATION OF AREA CHANGE

As the results produced by most methods of strain analysis (including those used here) are influenced by the amount of dilation, although we cannot determine this value, an independent method was applied to estimate area change. The population densities of zircons were counted for all areas around the leucosome in the *XZ* plane (Fig. 7).

Zircon distribution around the leucosome is clearly heterogeneous, although on a scale larger than that chosen for strain analysis. The lower mesosome has up to four times the zircon density of the upper mesosome, where the highest densities are in the vicinity of the melanosome. Zircon density also decreases from left to right, towards the tip of the leucosome.

Very constant values (24–56 zircons cm^{-2}, Fig. 7) were found in the area to the right of the leucosome tip, over the whole width (*Z* direction) of the studied sample, irrespective of the zircon densities in the laterally

a.

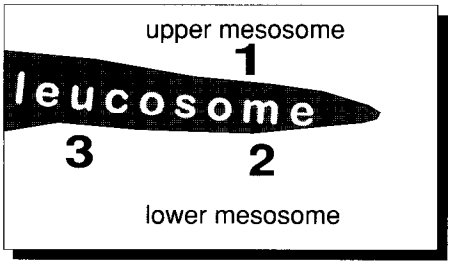

c.

grain	strain ratios determined by March analysis of sillimanite needle orientation	R_i of the cordierite core outline shape
1	1.17	1.10
2	2.83	3.06
3	6.38	6.52

b.

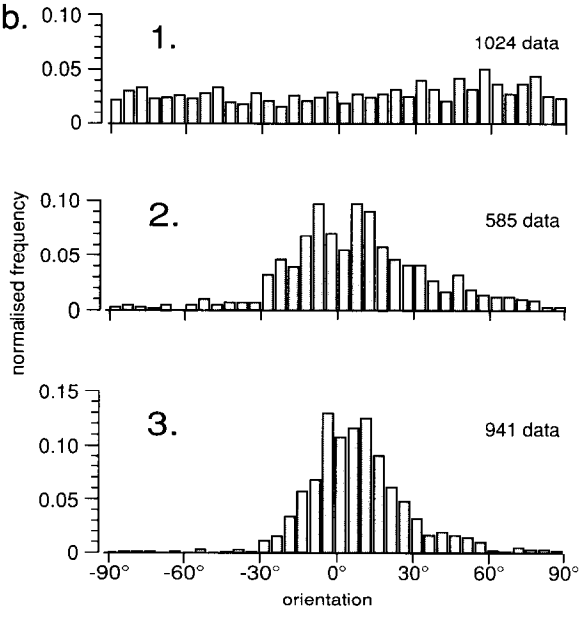

Fig. 6. Results of the March strain analysis on sillimanite grain orientation in three cordierite grains (see Fig. 3c & d for grains 1 and 2, respectively). (a) Relative position of the three cordierite grains (*XZ* plane). (b) Histograms of normalized frequency against sillimanite orientation (5° divisions) for the three examples. (c) Table of strain ratios obtained by March analysis of sillimanite orientation compared with the finite shape ratio of the individual cordierite core outlines.

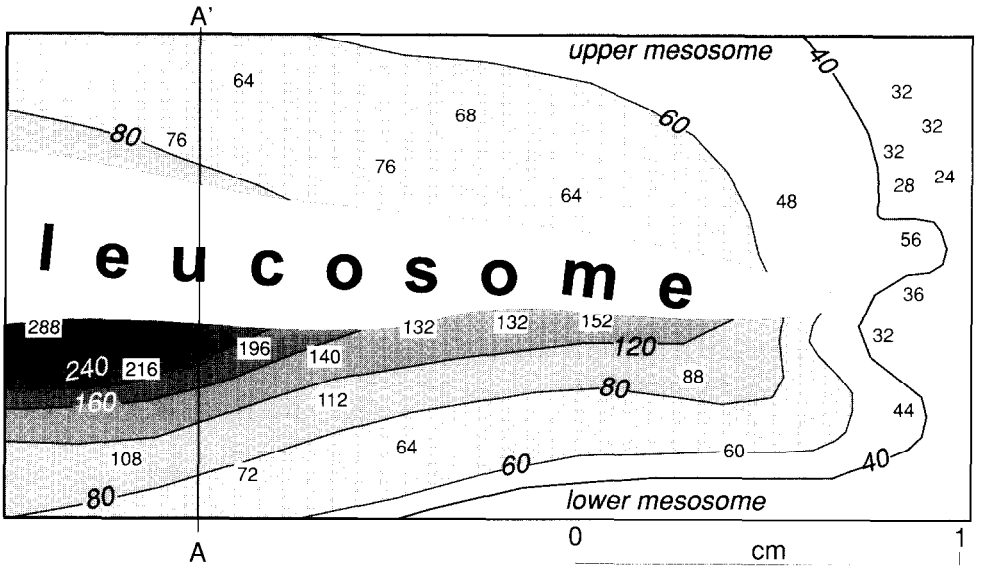

Fig. 7. Map of zircon population density in the XZ plane of the sample studied. Numbers represent zircons per cm^2. Subareas analysed are 5 × 5 mm. Isolines represent equal densities of zircons. A–A′ is the section line in Fig. 8.

equivalent zones above or below the leucosome. We propose that this area of the sample can be used to give a background zircon density for the gneiss, and reflects the situation before leucosome production and associated local dilation. Consequently, other densities around the leucosome can be converted to percentage area change (Δ_A%) using

$$\Delta_A\% = \left(\frac{b}{p} - 1\right) \times 100,$$

where b is the background value and p the zircon density at any point.

Interpreted in this way, the zircon density pattern suggests far more material was lost from the lower mesosome than from the upper mesosome, with the highest losses in the melanosome. Therefore, the term 'melanosome', although only texture descriptive, can be defined here as a region of more than 35% area loss. Material loss was not high enough in the upper mesosome to produce such a feature. Note also two lobes of area loss which extend from the tip of the leucosome into the upper and lower mesosomes.

For the following reasons we propose that the causes of the area loss was partial melt lost from the mesosomes and melanosome to form the leucosome. First, the leucosome contained true melt (see discussion of the evidence below). Second, the highest zircon densities correspond to areas enriched in refractory minerals (the melanosome); and, third, zircon densities are constant to the right of the leucosome.

If a traverse is taken across the sample, converting zircon density into area change (Fig. 8), the integral of the region under the area-change curve (assuming the leucosome represents 100% area increase) is zero. The area loss of the areas above and below the leucosome was integrated using Simpson's Law for estimating the volume under a three-dimensional surface (calculation made with the software programme SURFER, ©Golden Software Inc.). The integral sum of the area loss amounts to 145% of the area gain within the leucosome. Therefore, in terms of melt, we consider the leucosome and its immediate surrounding area to approximate to a closed system.

DISCUSSION

Strain paths of the various migmatite bodies

A strain path demonstrates the strain of a body during deformation (Elliott, 1972; Means, 1976; Flinn, 1978). Such a path can be constructed using markers which have recorded different increments of the strain history. Zircon position fabrics reflect the highest strain and, if the zircons are detrital in this paragneiss, then these fabrics

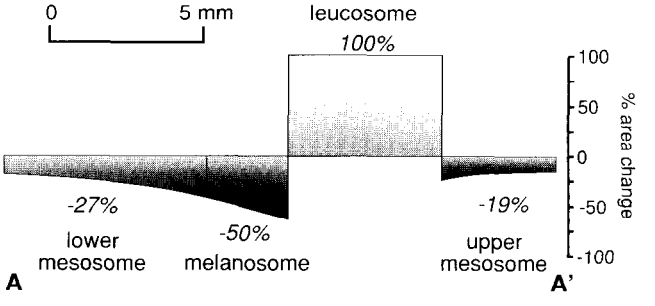

Fig. 8. Traverse across the leucosome along the line A–A′ (Fig. 7), showing the per cent of area change. Numbers in italics show the average area change of each area around the leucosome.

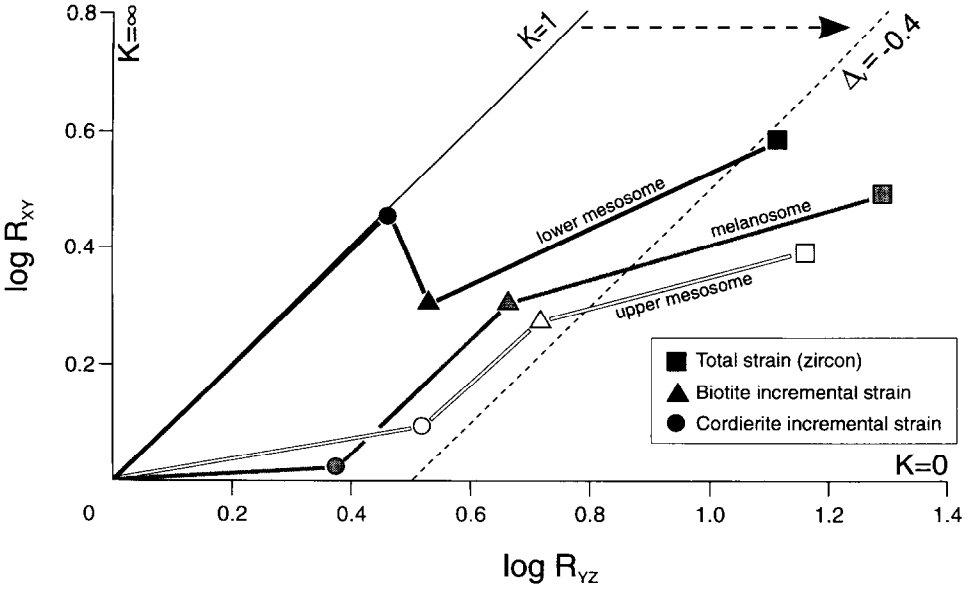

Fig. 9. Logarithmic Flinn plot of all the strain results, with inferred strain paths. The dashed line represents the $K = 1$ line after volume loss of $\Delta_v = -0.4$ (see text).

reflect the total finite strain. Cordierite and biotite are clearly reaction products of the low-pressure regional metamorphism and were therefore only markers from some stage during D_3 deformation until the end of the deformation. Assuming progressive pure shear, each strain increment can be removed from the final strain to find the point at which this marker first began to record strain. We consider this to be by far the best method for the construction of strain paths as much more complex methods are required for non-coaxial strain history paths, for which we had no evidence for or against.

The strain increment points can be tentatively connected to form strain paths for each area of the migmatite. Figure 9 shows the strain paths on a logarithmic Flinn plot. Such a plot has the advantage over a normal Flinn plot, in that strain paths with constant K values follow straight lines (e.g. Ramsay, 1967; Ramsay and Huber, 1983, p. 178).

All three strain paths lie below the $K = 1$ line in the apparent flattening field but follow different courses. Error in the strain measurements does not allow individual paths to be compared in detail with each other, but clearly each migmatite body follows a slightly different (K) path, and the various markers in each body began to record strain at approximately the same amounts of finite strain. Ignoring the cordierite data because they might not represent the true matrix strain (see above), the strain paths in Fig. 9 follow relatively straight lines.

The interplay of area/volume change and strain

It would be possible to identify the apparently flattening strain paths in Fig. 9 as the results of (plane) strain accompanied by incremental volume loss (Ramsay and Wood, 1973, fig. 4; Hobbs *et al.*, 1976, fig. 1.22). Following this scenario, the total volume loss would be least 40%, being highest in the melanosome and upper mesosome (Fig. 9). This does not agree with the XZ area change results (Fig. 7).

We envisage that as the leucosome developed the migmatite bodies underwent strain paths similar to those in Fig. 9, but the interplay of true strain and deviatoric volume change does not allow these individual components to be deciphered. Consider the following evidence.

(1) The apparent strain zircon position fabrics (Fig. 9) are a product of true strain plus (deviatoric) volume change, as only partly seen by absolute area changes in the XZ plane (Fig. 7), together with an unknown quantity of material transfer in the Y direction.

(2) From Fig. 4, zircon position strain values in the area to the right of the major bodies around the leucosome, an area designated in the area change analysis as 'the background value', are much lower than their counterparts to the left. However, area loss (Figs 7 & 8) could only account for the difference in R_f values obtained in the melanosome and its counterpart area (requiring approximately 40–50% material loss in the Z direction only). In the lower and upper mesosome the area loss (Fig. 8; 19 and 27%, respectively) cannot account for the lateral differences in strain, therefore suggesting the strain differences in these areas are, at least partly, real.

The leucosome; melt or solid-state material transfer?

The following lines of evidence demonstrate the material in the leucosome was true melt.

Table 3. A statistical comparison of zircons from the leucosome and mesosome. Grain-section areas are given for the *XZ* plane

Area	Minimum/maximum length to width ratio	Mean length to width ratio/σ_n	Mean grain area ($\times 10^3$ μm^2)/σ_n
Mesosome ($n=75$)	1.07/4.01	2.49/0.7	3.76/2.9
Leucosome ($n=42$)	1.66/11.25	3.69/1.5	1.09/0.9

σ_n, standard deviation.

(1) Zircons from the mesosomes and leucosome were examined using a U-stage microscope (Table 3). Mesosome zircons are large and round, with ill-defined grain surfaces (e.g. Fig. 3f). This is typical of metamorphic or detritic zircons (Mager, 1981; Trautnitz, 1982). In comparison, zircons within the leucosome are smaller (Table 3), but with a larger length/width ratio and well-developed crystal faces, especially prism and pyramid surfaces (Fig. 3e). We suggest that because the leucosome zircons are smaller (therefore ruling out simple overgrowth by metamorphic fluids, cf. Wayne and Sinha, 1988), but have better developed crystal shape, these are new magmatic zircons that grew in the leucosome melt.

(2) Minerals such as biotite and microcline, in particular when neighbouring quartz, show well-developed crystal faces and 120° triple-point boundaries in the leucosome but not in the mesosome (Fig. 3a & b). This is additional evidence for crystal growth in melt (Vernon and Collins, 1988).

(3) The nearly random distribution of poles to the (001) plane of biotite in the leucosome (Fig. 10a; see also the March analysis of leucosome biotite) compared with those, for instance, in the melanosome or mesosome (Fig. 10b) also demonstrates that solid-state deformation did not affect the leucosome. The leucosome biotite texture is comparable to that of a granite (e.g. Turner and Weiss, 1963).

Evidence of melt deformation in the leucosome

The magmatic and near-random textures of the leucosome (e.g. Fig. 10a) show that it cooled and crystallized after the end of the deformation of the studied sample. Melt deformation in the leucosome is reflected by the orientation of the *c*-axes of leucosome zircons (Fig. 11a). These show a strong preferred orientation pattern, similar to that of the mesosome (Fig. 11b). However, it is impossible to quantify (e.g. with the March analysis) the amount of 'fluid deformation' that took place in the leucosome during deformation: first, because the leucosome zircons (Table 3) have variable length/width ratios and therefore would rotate at different velocities during deformation (Jeffreys, 1923); and, second, because of the small number of leucosome zircons.

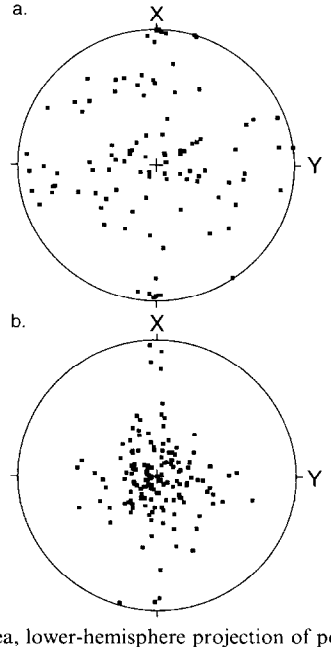

Fig. 10. Equal-area, lower-hemisphere projection of poles to the (001) plane of biotites in (a) the leucosome ($n=55$) and (b) the melanosome ($n=128$). The perimeter of the net is the *XY* plane.

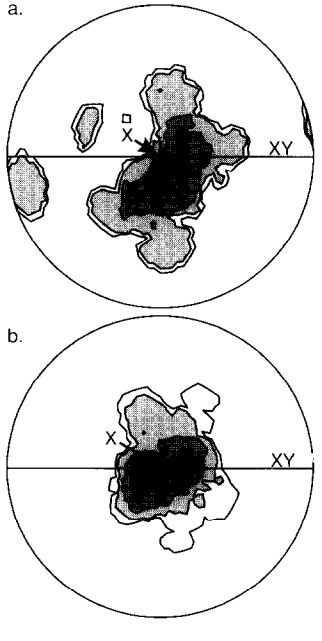

Fig. 11. Equal-area, lower-hemisphere projections of the orientation of the zircon *c*-axes in (a) the leucosome and (b) the lower mesosome. Contours at 1, 1.8, 5 and 9.3% uniform distribution.

INTERPRETATION

The development of foliation-parallel leucosomes is controversial, although they are very common features of gneiss terrains. Our data demonstrate that the leucosome developed parallel to the foliation plane. In a paragneiss, that was already foliated, local melt, mainly produced in the lower mesosome, migrated into a fracture between the upper mesosome and the melanosome. The apparent migration of the leucosome tip towards the right is shown by the corresponding increase in the amount of area loss in the adjacent gneiss.

From their experimental work, Dell'Angelo and Tullis (1988) showed that cataclastic behaviour and fracturing may occur in migmatites at very high strain rates and significant (> 15%) melt contents, as the result of elevated pore pressure. At the same time, the same authors are of the opinion that foliation-parallel leucosomes should not develop because extensional fractures cannot be formed in this orientation. McLellan (1988) explains foliation-parallel leucosomes from the Boca de Quadra in Alaska by a boudinage process. In our example this is clearly not the case. Maaløe (1992), in an investigation of the migmatites in the Østfold region of Norway, suggested material filled a shear fracture that developed parallel to foliation by diffusive transport in the presence of melt. However, in contrast to our work, Maaløe (1992) proposes the leucosome must develop symmetrically, where two melanosomes evolve around the leucosome.

Grujic and Mancktelow (1997) and in personal communication (1997) infer from pure-shear experiments that leucosomes may start as weak, subrounded melt objects that localize shear zones at their tips oriented at 45° with respect to the XY plane of strain. The shear zones will rotate passively towards the bulk XY plane with strain. However, this model is not applicable to our example, where leucosomes, over their whole length, are always parallel with the foliation.

Hand and Dirks (1992), in their model explaining axial-planar growth of leucosomes in crenulations, suggested that originally spherical leucosomes grew passively by diffusion-controlled melt migration into parallelism with the σ_2–σ_3 plane of stress, due to the action of differential stresses set up in the leucosome wall. Similarly, Jaeger and Cook (1979) suggested that in a simple-shear regime, if the tip of the fracture is elliptical, the highest (magnified) tangential stresses along the wall of the fracture are at a very acute angle to the foliation. Given that the foliation is the weakest plane in the foliated gneiss (cf. Wickham, 1987), a fracture will tend to grow actively along the foliation. Tanner (1996) adopted this model for the development of stromatitic leucosomes and suggested that the influx of melt into the fracture opposes the compressive stresses which will tend to close the fracture.

We further suggest that the fracture was a shear fracture, because only the zircon position fabrics in the subarea to the right of the leucosome–melanosome suggest the long axis of the XZ ellipse is oriented at 25° to the foliation (Fig. 4). This indicates that a 'bead' of localized ductile shear may have formed in advance of the propagating tip of the leucosome-bearing fracture.

CONCLUSIONS

In the gneiss studied, melt is concentrated in a foliation-parallel leucosome. The leucosome developed in a closed system, i.e. the leucosome melt originated from the immediately surrounding area. Melt was derived heterogeneously from the gneiss around the leucosome; most came from the lower mesosome and led to the development of the melanosome only in this area.

Strain and strain paths of the various migmatite areas, recorded by different strain markers, also vary around the leucosome. The apparent flattening strain in all the areas is probably the result of deviatoric volume loss and true strain increments, but these components cannot be further identified with the available information. The leucosome was also deformed in the molten state, but did not crystallize until the end of the deformation.

Acknowledgements—We thank Djordje Grujic, Patrick O'Brien and Johannes Schuster for useful discussions and their comments. Paul Dirks, Lisa Dell'Angelo, Sue Treagus, Win Means and an unknown reviewer suggested improvements to the manuscript. During the course of this research DCT received a grant from the DAAD (German Academic Exchange Service) and an additional fieldwork grant from the Ampthill and Meppershall Church Foundation.

REFERENCES

Ashworth, J. R. (1979) Comparative petrography of deformed and undeformed migmatites from the Grampian Highlands of Scotland. *Geological Magazine* **116**, 445–456.

Ashworth, J. R. (1985) Introduction. In *Migmatites*, ed. J. R. Ashworth, Blackie, Glasgow, pp. 1–35.

Atherton, M. P. and Gribble, C. D. (eds) (1983) *Migmatites, Melting and Metamorphism*. Shiva, Natwich.

Behrmann, J. H., O'Brien, P., Tanner, D. C. and Schuster, J. (1994) Heat and motion during late Variscan mountain building in the Moldanubian of Bavaria. *Journal of the Czech Geological Society* **39**, 8–9.

Blümel, P. (1982) Aufbau, Metamorphose, und geodynamische Deutungen des Variszischen Grundgebirges im Bereich der Bundesrepublik. *Jahrbuch der Ruhr-Universität Bochum* **1982**, 169–201.

Blümel, P. (1986) Metamorphic processes in the Variscan crust of the central segment. In *Proceedings of the 3rd Workshop on the European Geotraverse (EGT) Project: The Central segment*, eds R. Freeman, S. Mueller and P. Giese, European Science Foundation, Strassbourg, pp. 149–155.

Davis, G. L. and Schreyer, W. (1962) Alterbestimmung an Gesteinen des ostbayerischen Grundgebirges und ihre geologische Bedeutung. *Geologische Rundschau* **52**, 146–169.

Dell'Angelo, L. N. and Tullis, J. (1988) Experimental deformation of partially melted granitic aggregates. *Journal of Metamorphic Geology* **6**, 495–516.

Dunnet, D. (1969) A technique of finite strain analysis using elliptical particles. *Tectonophysics* **7**, 117–136.

Elliott, D. (1972) Deformation paths in structural geology. *Bulletin of the Geological Society of America* **83**, 2621–2638.

Erslev, E. A. (1988) Normalized center-to-center strain analysis of packed aggregates. *Journal of Structural Geology* **10**, 201–209.

Erslev, E. A. and Ge, H. (1990) Least-squares center-to-center and mean object ellipse fabric analysis. *Journal of Structural Geology* **12**, 1047–1059.

Fediuk, F. (1974) Cordieritregelung in moldanubischen Gneisen. *Krystalinikum* **10**, 79–88.

Flinn, D. (1969) Grain contacts in crystalline rocks. *Lithos* **3**, 361–370.

Flinn, D. (1978) Construction and computation of three-dimensional progressive deformations. *Journal of Geological Society of London* **135**, 291–305.

Foye, W. G. (1916) Are the 'batholiths' of the Haliburton–Bancroft area, Ontario, correctly named? *Journal of Geology* **24**, 783–791.

Fry, N. (1979) Random point distribution and strain measurements in rocks. *Tectonophysics* **60**, 89–106.

Grauert, B., Grosse-Westermann, U. and Albat, F. (1990) Interpretation von U–Pb-Monazitaltern moldanubischer Gneise. *KTB Report* **90**, 548.

Grauert, B., Hänny, R. and Soptrajanova, G. (1973) Age of origin of detrital zircons from the pre-Permian basement of the Bohemian Massif and the Alps. *Contributions to Mineralogy and Petrology* **40**, 105–130.

Grujic, D. and Mancktelow, N. S. (1997) High-grade shear zones: analogue experiments and comparison with examples from Southern Madagascar. *Terra Abstracts* **9**, 173.

Hand, M. and Dirks, P. H. G. M. (1992) The influence of deformation on the formation of axial planar leucosomes and the segregation of small melt bodies within the migmatitic Napperby Gneiss, central Australia. *Journal of Structural Geology* **14**, 591–604.

Hobbs, B. E., Means, W. D. and Williams, P. F. (1976) *An Outline of Structural Geology*. John Wiley & Sons, New York.

Jaeger, J. C. and Cook, N. G. W. (1979) *Fundamentals of Rock Mechanics*. Chapman and Hall, London.

Jeffreys, G. B. (1923) The motion of elliptical particles immersed in a viscous fluid. *Proceedings of the Royal Society of London* **A102**, 161–177.

Jurewicz, S. R. and Watson, E. B. (1985) The distribution of partial melt in a granitic system: the application of liquid phase sintering theory. *Geochimica et Cosmochimica Acta* **49**, 1109–1121.

Karlsson, G. and Wahlgren, C. H. (1982) A statistical investigation of grain contacts in a migmatite. *Neues Jahrbuch für Mineralogie, Monatshefte* **H8**, 348–360.

Kleemann, U. (1992) Petrologische Hinweise für einen tektonischen Versatz von Paläogeothermen am Westrand der Böhmischen Masse (NE Bayern). *Frankfurter geowissenschaftliche Arbeiten* **A11**, 82–85.

Kreuzer, H., Seidel, E., Schlüssler, U., Okrusch, M., Lenz, K.-L. and Raschka, H. (1989) K–Ar geochronology of different tectonic units at the northwestern margin of the Bohemian Massif. *Tectonophysics* **157**, 149–178.

Lindh, A. and Wahlgren, C.-H. (1985) Migmatite formation at subsolidus conditions—an alternative to anatexis. *Journal of Metamorphic Geology* **3**, 1–12.

Lisle, R. (1985) *Geological Strain Analysis: A Manual for the Rf/phi Method*. Pergamon Press, Oxford.

Loberg, B. (1963) The formation of flecky gneiss and similar phenomena in relation to the migmatite and veined gneiss problem. *Geologiska Föreningens i Stockholm Förhandlingar* **85**, 3–109.

Maaløe, S. (1992) Melting and diffusion processes in closed-system migmatization. *Journal of Metamorphic Geology* **10**, 503–516.

Mager, D. (1981) Vergleichende morphologische Untersuchungen an Zirkonen des altkristallinen Augengneises von Sand in Taufers (Südtirol) und einiger benachbarter Gesteine. *Neues Jahrbuch für Mineralogie, Monatshefte* **H9**, 385–397.

March, A. (1932) Mathematische Theorie der Regelung nach der Korngestalt bei affiner Deformation. *Zeitschrift für Kristallographie* **81**, 285–297.

McKenzie, D. (1984) The generation and compaction of partially molten rock. *Journal of Petrology* **25**, 713–765.

McKenzie, D. (1985) The extraction of magma from the crust and mantle. *Earth and Planetary Science Letters* **74**, 81–91.

McLellan, E. L. (1983) Contrasting textures in metamorphic and anatectic migmatites: an example from the Scottish Caledonides. *Journal of Metamorphic Geology* **1**, 241–262.

McLellan, E. L. (1988) Migmatite structures in the Central Gneiss Complex, Boca de Quadra, Alaska. *Journal of Metamorphic Geology* **6**, 517–542.

Means, W. D. (1976) *Stress and Strain*. Springer, New York.

Mehnert, K. R. (1962) Zur Systematik der Migmatite. *Krystalinikum* **1**, 95–110.

Mehnert, K. R. (1968) *Migmatites and the Origin of Granitic Rocks*. Elsevier, Amsterdam.

Mehnert, K. R. and Büsch, W. (1982) The initial stage of migmatite formation. *Neues Jahrbuch für Mineralogie, Abhandlung* **145**, 211–238.

Mielke, H. (1990) *Geologische Karte von Bayern, Blatt Nr 6542 Untergrafereid und Blatt Nr 6642 Waldmünchen, mit Erlauterung*. Bayerisches Ecologisches Lundisant, München.

Niggli, P. and Huber, H. M. (1943) Physiographie und Genesis der Gesteine im südostlichen Gotthardmassiv. *Schweizerische Mineralogische und Petrographische Mitteilungen* **23**, 72–260.

O'Brien, P. J. (1989) The petrology of retrograded eclogites of the Oberpfalz Forest, northeastern Bavaria West Germany. *Tectonophysics* **157**, 195–212.

O'Brien, P. J. and Vrána, S. (1995) Eclogites with a short-lived granulite facies overprint in the Moldanubian Zone, Czech Republic: petrology, geochemistry and diffusion modelling of garnet zoning. *Geologische Rundschau* **84**, 473–488.

Oertel, G. (1985) Reorientation due to grain shape. In *Preferred Orientation in Deformed Metals and Rocks: An Introduction to Modern Texture Analysis*, ed H. R. Wenk, Academic Press, Orlando. pp. 259–265.

Olsen, S. N. (1982) Open- and closed-system migmatites in the Front Range Colorado. *American Journal of Science* **282**, 1596–1622.

Passchier, C. W. (1990) Reconstruction of deformation and flow parameters from deformed vein sets. *Tectonophysics* **180**, 185–199.

Ramsay, J. G. (1967) *Folding and Fracturing of Rocks*. McGraw-Hill, New York.

Ramsay, J. G. and Huber, M. I. (1983) *The Techniques of Modern Structural Geology. Volume 1: Strain Analysis*. Academic Press, London.

Ramsay, J. G. and Wood, D. S. (1973) The geometric effects of volume change during deformation processes. *Tectonophysics* **13**, 263–277.

Robin, P.-Y. F. (1979) Theory of metamorphic segregation and related processes. *Geochimica et Cosmochimica Acta* **43**, 1587–1600.

Sawyer, E. W. and Barnes, S.-J. (1988) Temporal and compositional differences between subsolidus and anatectic migmatite leucosomes from the Quentico metasedimentary belt Canada. *Journal of Metamorphic Geology* **6**, 437–450.

Schuster, J. (1994) Metamorphism evolution of the Moldanubian zone of the Oberpfälzer Wald/NE Bavaria. *Journal of the Czech Geological Society* **39**, 99.

Skrotzki, W. and Siegesmund, S. (1992) Mechanismus der Verformung und Texturentwicklung in Cordieriten aus moldanubischen Gneisen. *Frankfurter Geowissenschaftliche Arbeiten* **A11**, 163.

Skrotzki, W., Weber, K. and Müller, W. F. (1992) Gefügekundliche Untersuchungen im KTB mittels TEM. *KTB Report* **92**, 261–276.

Tanner, D. C. (1996) Strukturen und Gefüge in hochgradig metamorphen Gneisen der mittleren Oberpfalz und Westböhmens. *Giessener Geologische Schriften* **57**, 1–198.

Tanner, D. C. and Behrmann, J. H. (1995) The Variscan tectonics of the Moldanubian gneisses, Oberpfälzer Wald: a compressional history. *Neues Jahrbuch für Geologie und Paläontologie, Abhandlung* **197**, 331–355.

Tanner, D. C., Schuster, J., Behrmann, J. H. and O'Brien, P. J. (1993) New clues to the Moldanubian puzzle: structural and petrological observations from the Waldmünchen area, eastern Bavaria. *KTB Report* **93**, 97–102.

Teufel, S. (1988) Vergleichende U–Pb- und Rb Sr-Altersbestimmungen an Gesteinen des Übergangsbereiches Saxothuringikum/Moldanubikum, NE Bayern. *Göttinger Arbeiten zur Geologie und Paläontologie* **35**, 1–87.

Tondar, P. and Troll, G. (1992) Zircon typology of Moldanubian leptynites of Passauer Wald (Bavaria): a key to their origin. In *Proceedings of the 1st International Conference on the Bohemian Massif, Prague, Czechoslovakia*, ed. Z. Kukal, Czech Geological Survey, Prague. pp. 316–319.

Trautnitz, H.-M. (1982) Zirkonstratigraphie nach vergleichender morphologischer Analyse und statistischen Rechnenverfahren—dargestellt am Beispiel klastischer Gesteine im Harz. Diploma thesis, Universität Erlangen.

Turner, F. J. and Weiss, L. E. (1963) *Structural Analysis of Metamorphic Tectonics*. McGraw-Hill, New York.

Unzog, W. (1992) *STRAIN v5/92. A Collection of Strain Analysis Programs*, Unpublished software program. Graz.

van Roermund, H. L. M. and Konert, R. J. (1990) Deformation and recrystallisation mechanisms in naturally deformed cordierite. *Physics and Chemistry of Minerals* **17**, 52–61.

Vernon, R. H. and Collins, W. J. (1988) Igneous microstructures in migmatites. *Geology* **16**, 1126–1129.

Voll, G. (1960) Stoff, Bau und Alter in der Grenzzone Moldanubikum/ Saxothuringikum in Bayern unter besonderer Berücksichtigung gabbroider, amphibolitischer und kalksilikatführender Gesteine. *Beihefte zum Geologischen Jahrbuch* **42**, 382.

Wagener-Lohse, C. and Blümel, P. (1986) Prograde Niederdruckmetamorphose und ältere Mitteldruckmetamorphose im Nordostbayerischen Abschnitt der Grenzzone Saxothuringikum/ Moldanubikum. In *76 Jahrestagung der geologische Vereinigung, Gießen*. Geologische Vereinigung, Mendig. pp. 84–86.

Wayne, D. M. and Sinha, K. A. (1988) Physical and chemical response of zircons to deformation. *Contributions to Mineralogy and Petrology* **98**, 109–121.

Wickham, S. M. (1987) The segregation and emplacement of granitic magmas. *Journal of Geological Society of London* **144**, 281–297.